

Scattering Suppression in a 4G and 5G Base Station Antenna Array Using Spiral Chokes

Hai-Han Sun [✉], Member, IEEE, He Zhu [✉], Member, IEEE, Can Ding [✉], Member, IEEE, Bevan Jones, Life Member, IEEE, and Y. Jay Guo [✉], Fellow, IEEE

Abstract—This letter presents a novel distributed choking technique, the spiral choke, for scattering suppression in dual-band antenna arrays. The working principle and the scattering suppression capability of the choke are analyzed. The spiral chokes are implemented as low-band radiators in a colocated 4G and 5G dual-band array to suppress cross-band scattering while broadening the bandwidth of the choked element. The experimental results demonstrate that the cross-band scattering in the array is largely eliminated, and the realized dual-band array has very stable radiation performance in both well-matched bands.

Index Terms—Base station antennas (BSA), 4G, 5G, choking techniques, cross-band scattering suppression, dual-band arrays.

I. INTRODUCTION

NOWADAYS, there is a concerted international effort to deploy the fifth-generation (5G) mobile communications networks. Owing to environmental and cost considerations, mobile operators expect 5G antenna arrays to be collocated to fourth-generation (4G) ones on the same panels, whilst no major degradation of antenna radiation patterns is allowed. However, the close spacing between elements at different bands often leads to strong cross-band scattering. Especially, elements operating in the low band (LB) usually present as large scatterers in the high band (HB), causing the distortion of HB radiation patterns and the reduction of the cross-band port isolation. The cross-band scattering problem has been a long-existing issue in multiband antenna arrays.

To suppress the cross-band scattering, the traditional method uses a variety of metal baffles or walls [1]–[4]. The shape, size, and position of metal baffles are optimized through trial and error to improve the radiation performance in both bands. Some reduction in cross-band scattering can be achieved, but the method adds design complexity especially when several different bands are involved.

Choking techniques have been presented to suppress cross-band scattering in dual-band arrays [5], [6]. This method modifies the LB radiator by inserting lumped chokes with LB-pass HB-stop property. As a result, the unwanted HB currents on

Manuscript received July 6, 2020; revised July 31, 2020, August 10, 2020, and August 14, 2020; accepted August 24, 2020. Date of publication August 27, 2020; date of current version October 6, 2020. This work was supported by the Australian Research Council (ARC) DECRA under Grant DE200101347. (*Corresponding author: Hai-Han Sun.*)

Hai-Han Sun is with the Nanyang Technological University, Singapore 639798 (e-mail: haihan.sun199403@gmail.com).

He Zhu, Can Ding, Bevan Jones, and Y. Jay Guo are with the University of Technology Sydney, Sydney, NSW 2007, Australia (e-mail: he.zhu@uts.edu.au; can.ding@uts.edu.au; bbjones@bigpond.net.au; jay.guo@uts.edu.au).

Digital Object Identifier 10.1109/LAWP.2020.3019930

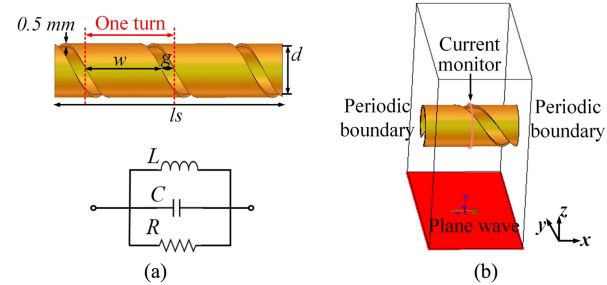


Fig. 1. (a) Configuration of the spiral structure and the equivalent circuit model. (b) Demonstration of the spiral illuminated by plane wave.

LB arms are minimized and the HB radiation patterns are restored. In [6], a dual-band array with choked LB element achieves low scattering and uncontaminated radiation performance in both bands. However, the inserted lumped chokes make the impedance matching of the choked antenna difficult. The achieved impedance bandwidth of the choked antenna is only 19.7% with $|S_{11}| < -10$ dB, which still fall short of the industrial requirements. Further investigations on the choking techniques are therefore needed to improve the bandwidth of the choked elements while having a good scattering suppression capability.

In this letter, we present a distributed choking structure, the spiral choke, as LB radiators to suppress HB scattering and broaden the bandwidth of choked LB antenna. The spiral structure has its intrinsic choking capability in the HB and operates like a dipole radiator in the LB, thus has negligible effects on the HB radiation while maintaining good matching capability in the LB. The spiral-choked LB element is employed in an interleaved dual-band base station antenna (BSA) array to demonstrate its performance. The array covers the 4G band from 1.71 to 2.26 GHz, and the 5G band from 3.3 to 3.7 GHz with excellent matching capability. With the spiral LB element implemented, the array achieves clean patterns with half-power beamwidth (HPBW) variation of $65^\circ \pm 5^\circ$ in both the high and low bands. The array demonstrates a practical solution to the industrial problem of colocating 4G and 5G antennas.

II. SPIRAL CHOKE

The configuration of the spiral structure is presented in Fig. 1(a). Similar to a helix coil, each cell of the spiral can be represented as a parallel RLC circuit. It acts as an open circuit at its resonant frequency where the impedance of the spiral goes to infinity, so an incident electric-field (E-field) cannot

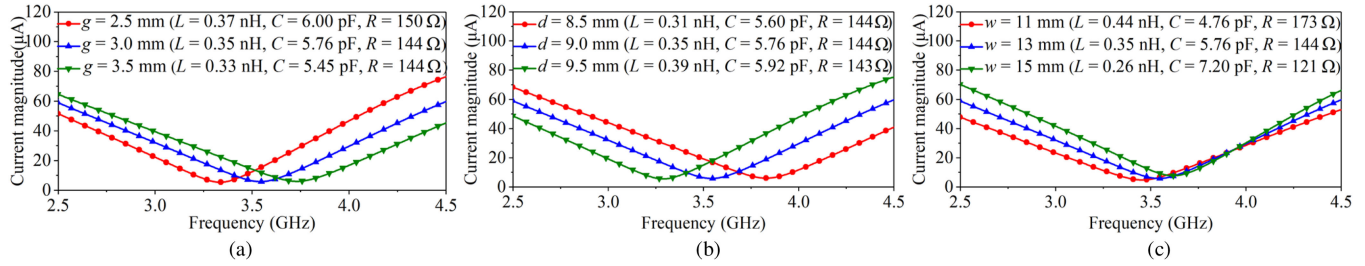


Fig. 2. Magnitude of the induced currents on the spiral structure with different values of (a) gap g , (b) inner diameter d , and (c) width of strip w . Other parameters of the spiral are $g = 3.0$ mm, $d = 9.0$ mm, and $w = 13.0$ mm unless specified in the plots. The thickness of the conductor is 0.5 mm.

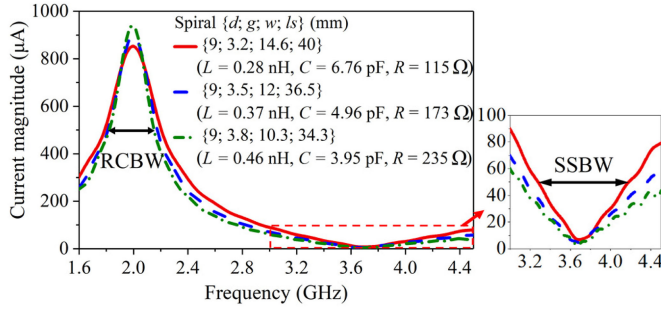


Fig. 3. Magnitude of the induced currents on the finite-length spiral structure that has an open-circuit resonance at 3.7 GHz and a short-circuit resonance at 2.0 GHz with different combinations of parameters.

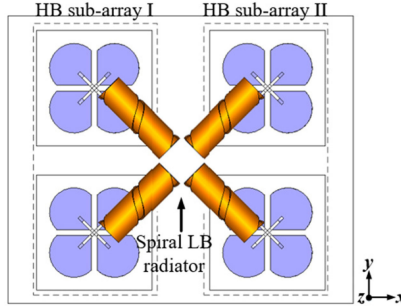


Fig. 4. Arrangement of the interleaved dual-band array with spiral LB radiators.

induce longitudinal currents. In the frequency bands that are much lower than the resonant point, it has a lower inductive impedance and a higher shunt capacitive impedance. It only introduces an additional small inductance compared with the corresponding cylindrical conductor, thus has a minimal effect on the radiator's impedance. The intrinsic property of the spiral makes it a distributed choke, which can be used as an LB radiator to suppress the unwanted induced HB currents while maintaining the radiating currents in the LB.

To study the ability of the spiral to suppress the HB currents, we need to find the resonant point of the spiral, which is the frequency where currents induced by an incident E-field are minimized. Minimizing induced HB currents on the spiral minimizes the HB scattering. To achieve this, a single cell of the spiral with periodic boundary conditions at both ends is modeled, as shown in Fig. 1(b). It is illuminated by a plane wave with E-field

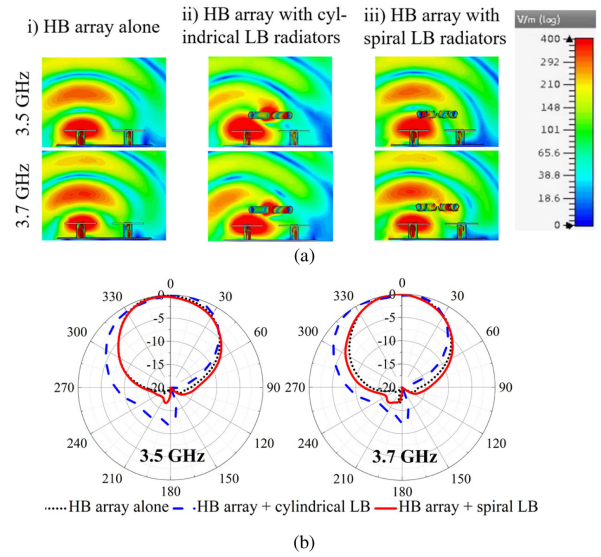


Fig. 5. Comparison of (a) electric-field cuts, and (b) normalized HB radiation patterns in the xz plane under the circumstances of: i) HB array alone, ii) HB array with cylindrical LB radiators, and iii) HB array with spiral LB radiators.

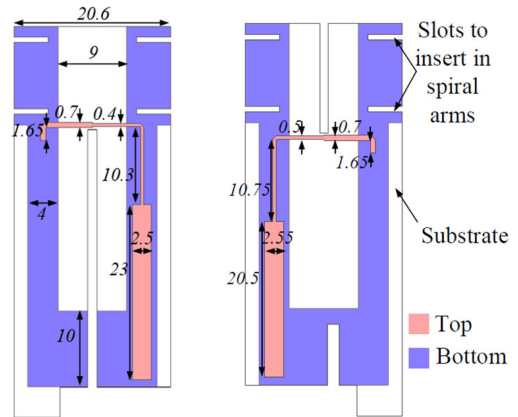


Fig. 6. Configurations of the two baluns for the spiral LB element. (The substrate is FR4 with dielectric constant of 4.4 and a thickness of 1.0 mm.)

along the axis of the spiral (x -axis), and currents induced on it are monitored. The periodic boundary is set to simulate an infinitely long spiral to eliminate the effects of discontinuities and to obtain general results that do not need to take account of the specific geometry of the antennas.

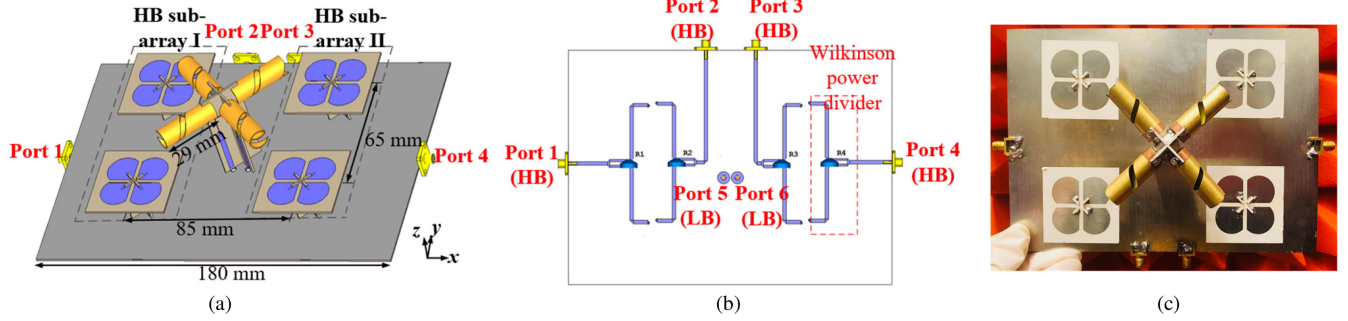


Fig. 7. (a) Perspective view of the dual-band antenna array model. (b) View of the feed network for the dual-band antenna array. (c) Front view of the fabricated antenna array prototype.

There are three important parameters for tuning the resonant frequency of the spiral: the distance between neighboring turns g , the inner diameter of spiral d , and the width of strip w . The induced currents flowing on the spiral structure with different values of g , d , and w are monitored and plotted in Fig. 2. The approximate values of distributed circuit components per millimeter of the spiral in different cases are extracted and listed in the figures. As shown in Fig. 2(a), a larger g moves the minimum current point to a higher frequency, corresponding to the spiral's resonant point moving to a higher frequency. This is because increasing g decreases both L and C , which in turn raises the parallel resonant frequency. Fig. 2(b) shows a larger d moves the resonant point to a lower frequency, as it increases both L and C . Fig. 2(c) shows a larger w moves the resonant point to a higher frequency, as it largely decreases L and only increases C to a smaller amount.

The spiral is implemented as LB radiators to suppress scattering currents in the HB while maintaining radiating currents in the LB. To examine its performance in high and low bands with different combination of parameters, we selected several finite-length spirals with an intrinsic open-circuit resonance at 3.7 GHz and a half-wavelength short-circuit resonance at 2.0 GHz, and compared the magnitudes of induced currents on them, as shown in Fig. 3. Here, we define the HB scattering suppression bandwidth (SSBW) and the LB radiating current bandwidth (RCBW) as the band in which the magnitude of current is less than $50 \mu\text{A}$ and higher than $500 \mu\text{A}$, respectively. Fig. 3 shows that a spiral with larger g and smaller w has a wider SSBW but has a slightly narrower RCBW. The spiral with a larger g and a smaller w has a smaller C and a larger L per unit length. Therefore, it is concluded that a larger L/C enhances the HB SSBW but reduces the LB RCBW. The optimization criteria of the spiral chokes as LB radiators are to effectively suppress the cross-band scattering in the HB while maintaining good matching and radiation performance in the LB.

III. IMPLEMENTATION OF THE SPIRAL CHOKE IN AN INTERLEAVED 4G AND 5G DUAL-BAND ANTENNA ARRAY

The spiral structure is implemented as LB radiators in a compact dual-band antenna array section to verify its performance, as shown in Fig. 4. Both the LB and HB radiators have the cross-dipole arrangement [7]–[9]. The LB element is located midway between two HB subarrays. The LB and HB antennas are designed to operate from 1.71 to 2.2 GHz, and from 3.3

to 3.7 GHz for the 4G and 5G operations, respectively. The parameters of the spirals are optimized to have a resonant point at 3.7 GHz as the distortion of HB patterns caused by the presence of unmodified LB element (cylindrical LB element) is more severe at frequencies around 3.7 GHz. The optimized parameters are $d = 9 \text{ mm}$, $w = 14.1 \text{ mm}$, and $g = 3.23 \text{ mm}$.

The E-field distribution and the radiation pattern of HB subarray I are investigated. The results in three cases are compared: i) HB array alone, ii) HB array with cylindrical LB arms, and iii) HB array with spiral LB arms, as shown in Fig. 5. Fig. 5(a) shows the E-field distributions in the horizontal section through the array. Compared with the case when only HB array is present, cylindrical LB radiators block the HB E-field to a large extent. The spiral LB radiators have much less effect on the HB E-field. The resultant horizontal patterns in these three cases are shown in Fig. 5(b). The deterioration of the HB radiation patterns in the presence of the cylindrical LB radiators has been largely eliminated using spiral LB arms, demonstrating the effectiveness of the spiral structure in reducing HB pattern distortion.

After demonstrating the effectiveness of the spiral structure in suppressing the cross-band scattering, the spiral radiators are matched by baluns which are designed following the guidelines in [10] and [11]. The configurations of the two baluns are shown in Fig. 6. They are orthogonally arranged to feed the two pairs of spiral arms. The spiral antenna is well-matched with reflection coefficients $< -15 \text{ dB}$ from 1.66 to 2.22 GHz. The radiation patterns of the spiral element are very stable across the band.

IV. EXPERIMENTAL RESULTS OF THE DUAL-BAND ARRAY

The configuration of the finalized dual-band array section is shown in Fig. 7. The spacings between HB elements in the designed array gives a minimum half-wavelength spacing at all frequencies for decorrelation in small cell multiple-input multiple-output (MIMO) antennas. The HB subarrays are fed by power dividers printed on the back of the reflector, and the LB element is fed by coaxial cables directly connected to the LB baluns. The array has been fabricated and tested.

The S -parameters of the HB subarray I are shown in Fig. 8. Fig. 8(a) and (b) shows the reflection coefficients and isolations, respectively. The measured bandwidth is 11.4% from 3.3 to 3.7 GHz for reflection coefficients $< -15 \text{ dB}$. The isolations between ports in the same subarray and in different subarrays are all $> 25 \text{ dB}$. The HB radiation patterns are plotted in Fig. 9. The $+45^\circ$ -polarized patterns for subarray I are presented. The results

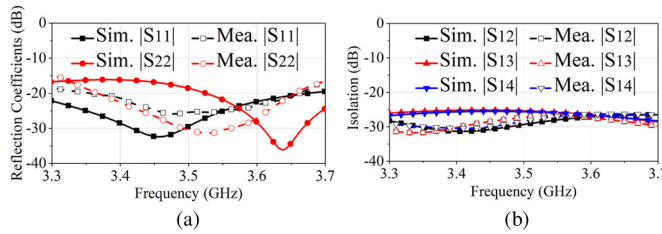


Fig. 8. Simulated and measured (a) reflection coefficients and (b) isolations for HB ports.

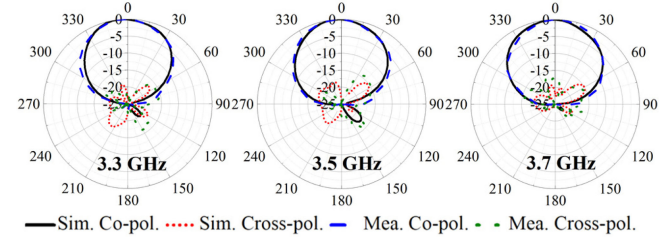


Fig. 9. Normalized horizontal radiation patterns for the HB subarray I.

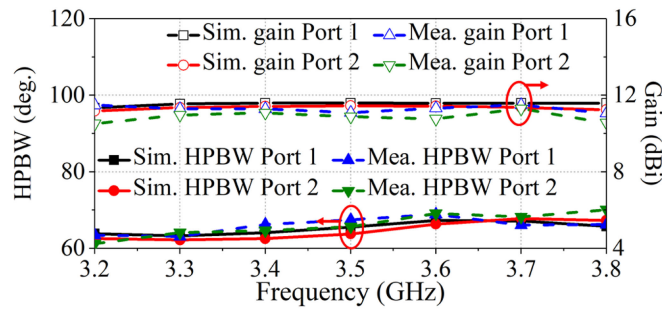


Fig. 10. Simulated and measured HPBW and gain for HB subarray I.

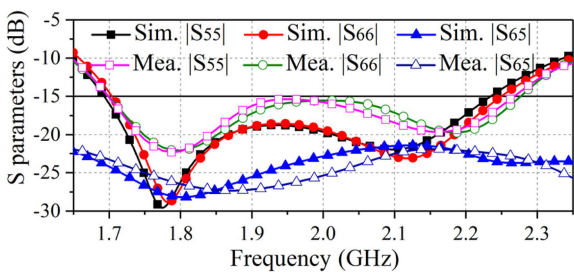


Fig. 11. Simulated and measured S-parameters for the spiral LB antenna.

for -45° polarization and for subarray II are almost identical with the presented results due to the symmetric geometry of the array configuration. The measured cross-polarization level is < -17 dB at the boresight. The radiation patterns are stable across the operating band with HPBWs of $66.5^\circ \pm 3.5^\circ$, which is shown in Fig. 10. Fig. 10 also shows that the measured gain of the HB subarray is around 11 dBi.

The results for the spiral LB element are shown in Figs. 11–13. Fig. 11 shows the reflection coefficients and isolation results. The measured bandwidth is 28.3% from 1.7 to 2.26 GHz for

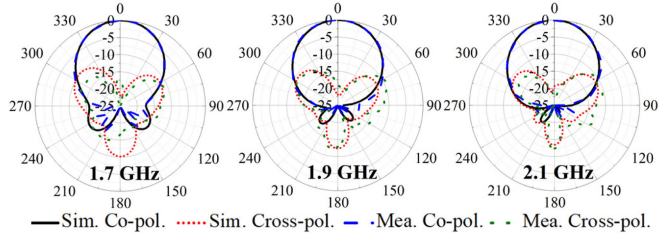


Fig. 12. Normalized horizontal radiation patterns for the spiral LB antenna.

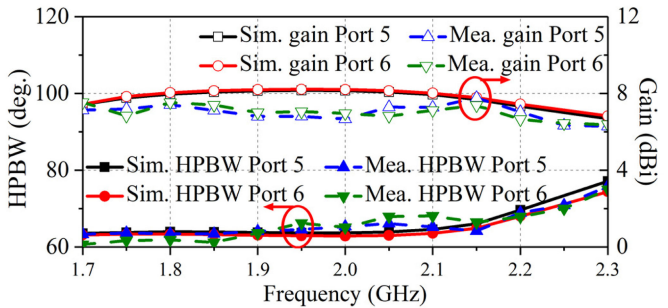


Fig. 13. Simulated and measured HPBW and gain for the spiral LB antenna.

reflection coefficients < -15 dB. The isolation between orthogonal ports is > 22 dB across the band, which is slightly lower than most of the cross-dipole antennas due to the coupled currents along slots in the spiral arms. Fig. 12 shows the LB radiation patterns of the $+45^\circ$ polarized radiation. The cross-polarization level is < -17 dB at the boresight. The horizontal HPBW and gain of the LB element are shown in Fig. 13. The LB radiation patterns are consistent with HPBWs of $65^\circ \pm 5^\circ$. The simulated and measured gains are around 8 and 7 dBi, respectively. The difference can be caused by the loss of the coaxial cables, and FR4 substrates of the baluns.

The implementation of spiral-choked LB element also improves the cross-band isolation in the HB but has negligible impact on the isolation in the LB. The copolarized and cross-polarized cross-band isolation in the HB is improved from -18 to -22 dB, and from -21 to -26 dB, respectively.

V. CONCLUSION

In this letter, a novel distributed choke, the spiral choke, is implemented in an interleaved 4G and 5G BSA array to minimize cross-band scattering. As a distributed choking structure, the spiral has intrinsic scattering suppression capability and helps to broaden the bandwidth of the choked LB antenna. The experimental results of the dual-band array demonstrate that the distortion of the HB pattern caused by the scattering from the cylindrical LB element is largely corrected with the spiral chokes. The spiral-choked LB element has a wider bandwidth with a better matching capability than the one in the previous work [6]. The presented dual-band array achieves stable radiation properties across well-matched HB and LBs with a simple and compact structure, which makes it highly suitable for the use in 4G and 5G BSA systems.

REFERENCES

- [1] H. Huang, Y. Liu, and S. Gong, "A novel dual-broadband and dual-polarized antenna for 2G/3G/LTE base stations," *IEEE Trans. Antennas Propag.*, vol. 64, no. 9, pp. 4113–4118, Sep. 2016.
- [2] H. Huang, Y. Liu, and S. Gong, "A dual-broadband dual-polarized base station antenna for 2G/3G/4G applications," *IEEE Antennas Wireless Propag. Lett.*, vol. 16, pp. 1111–1114, 2017.
- [3] Y. He, Z. Pan, X. Cheng, Y. He, J. Qiao, and M. M. Tentzeris, "A novel dual-band dual-polarized miniaturized and low-profile base station antenna," *IEEE Trans. Antennas Propag.*, vol. 63, no. 12, pp. 5399–5408, Dec. 2015.
- [4] Y. He, W. Tian, and L. Zhang, "A novel dual-broadband dual-polarized electrical downtilt base station antenna for 2G/3G applications," *IEEE Access*, vol. 5, pp. 15241–15249, 2017.
- [5] B. Jones, O. Isik, and C. Shang, "Dual-band interspersed cellular basestation antennas," EP Patent 2 769 476 B1, Dec. 24, 2012.
- [6] H. H. Sun, C. Ding, H. Zhu, B. Jones, and Y. J. Guo, "Suppression of cross-band scattering in multiband antenna arrays," *IEEE Trans. Antennas Propag.*, vol. 67, no. 4, pp. 2379–2389, Apr. 2019.
- [7] D. Su, D. Fu, T. N. C. Wang, and H. Yang, "Broadband polarization diversity base station antenna for 3G communication system," *J. Electromagn. Waves Appl.*, vol. 22, pp. 493–500, 2008.
- [8] H. Huang, Y. Liu, and S. Gong, "A broadband dual-polarized base station antenna with sturdy construction," *IEEE Antennas Wireless Propag. Lett.*, vol. 16, pp. 665–668, 2017.
- [9] Y. Cui, R. Li, and H. Fu, "A broadband dual-polarized planar antenna for 2G/3G/LTE base stations," *IEEE Trans. Antennas Propag.*, vol. 62, no. 9, pp. 4836–4840, Sep. 2014.
- [10] W. K. Roberts, "A new wide-band balun," *Proc. IRE*, vol. 45, pp. 1628–1631, Dec. 1957.
- [11] H. Sun, C. Ding, B. Jones, and Y. J. Guo, "A wideband base station antenna element with stable radiation pattern and reduced beam squint," *IEEE Access*, vol. 5, pp. 23022–23031, 2017.